Supplementary Information for

Sliding friction over individual covalent bonds correlates with bond order

Shinjae Nam[1†], Lukas Hörmann[2,3†], Oliver Gretz[1†], Oliver T. Hofmann[2], Franz J. Giessibl[1], Alfred J. Weymouth[1*]

Affiliations (plus present addresses):

[1]Faculty of Physics, University of Regensburg; Regensburg, 93053, Germany.

[2]Institute of Solid State Physics, Graz University of Technology; Graz, 8010, Austria.

[3]Now at the Institute of Chemistry, University of Warwick, Coventry, CV4 7AL, UK and Institute of Physics, University of Warwick, Coventry, CV4 7AL, UK

*Corresponding author. Email: jay.weymouth@ur.de

† These authors contributed equally to this work

This PDF file includes:

Materials and Methods

Experimental

In frequency-modulation LFM, the amplitude of oscillation is set, and the drive signal required to maintain this amplitude is recorded. If the drive signal increases, it indicates that there is energy loss during the tip's oscillation, referred to as energy dissipation. Energy dissipation (E_{diss}) represents the work done on the cantilever during one oscillation cycle and is measured in units of meV/cycle. This signal is recorded separately from the frequency shift (Δf, unit of Hz), which reflects the conservative interaction between the tip and the sample.

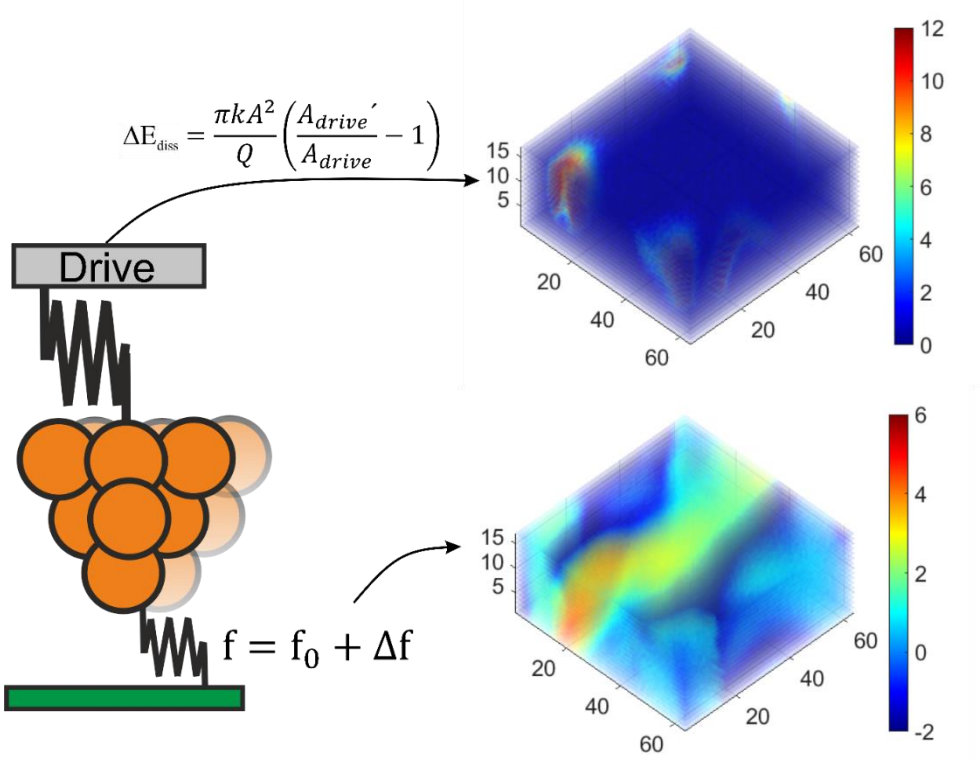

Supplementary Figure 1 | Simultaneously acquired data sets of conservative (Δf) and nonconservative (E_{diss}) interactions over OH bonds. The data is presented as a function of the lateral (x) and vertical (z) position of the tip, showing the spatial variation of interactions over the OH bonds.

Supplementary Figure 1 shows data sets of conservative and nonconservative interaction simultaneously acquired as a function of lateral (x) and vertical (z) position of the tip over the OH bonds. Two images of 3D data acquired above CC bonds are shown in Supplementary Figure 2. The Δf image corresponding to the data shown in Fig. 1c is shown in Supplementary Figure 3.

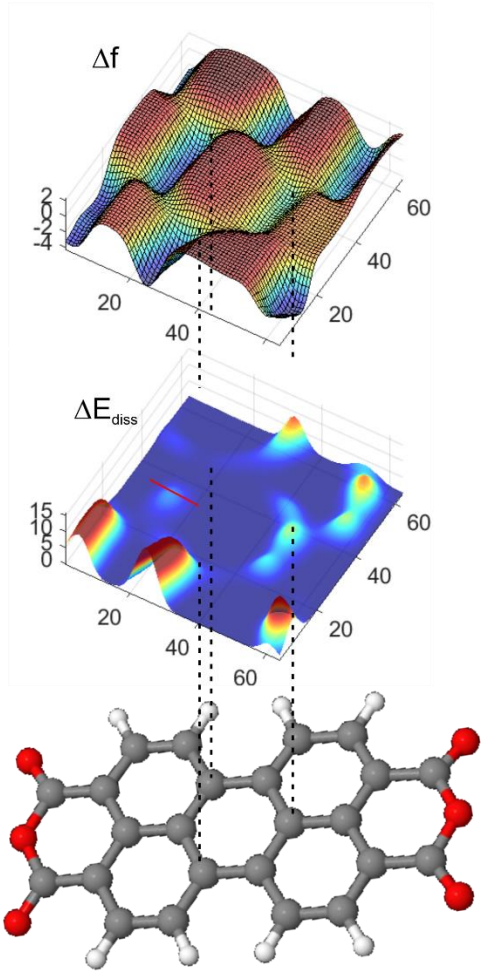

Supplementary Figure 2 | 2D images of energy dissipation (E_{diss}, in meV/cycle) and frequency shift (Δf, in Hz) acquired above CC bonds.

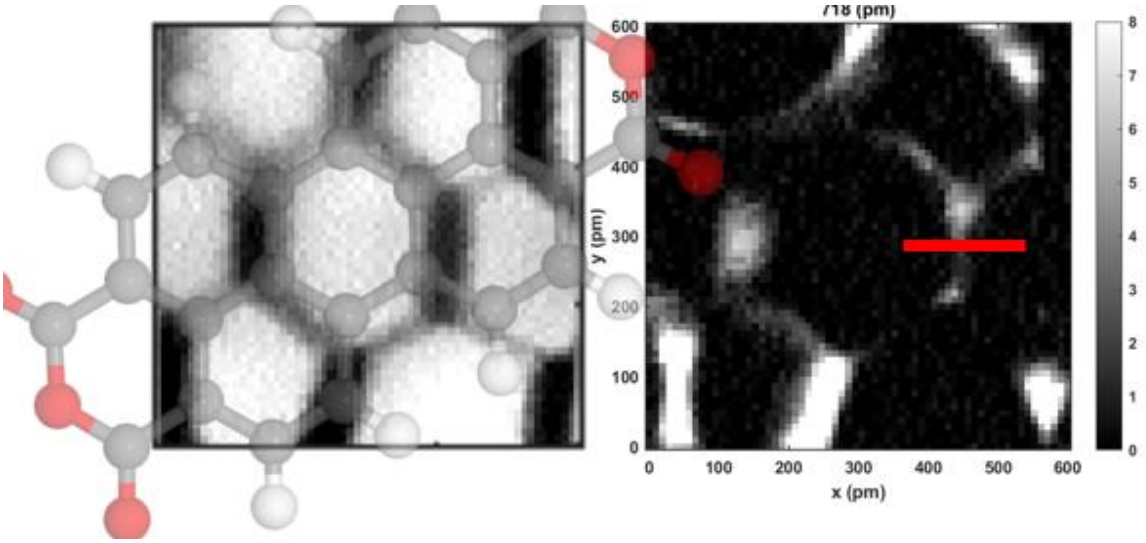

Supplementary Figure 3 | LFM frequency shift (Δf) and the E_{diss} signal of Fig. 1c (color axis is limited here to 8 meV/cycle to better show other bonds).

To compare the energy dissipation characteristics of different chemical bonds, the data were analyzed by plotting only the maximum values of the line scans shown in Supplementary Figure 4 as a function of tip height.

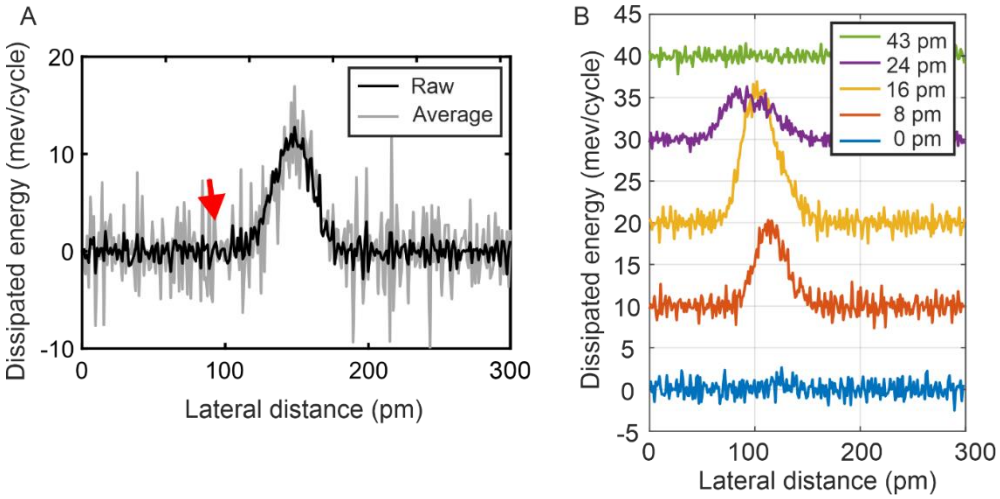

Supplementary Figure 4 | Analysis of E_{diss} data acquired over the chemical bonds. (A) Raw data of E_{diss} (gray line) recorded along the red line shown in Supplementary Figure 2. The red arrow indicates the position where the force hysteresis loop begins to open. To reduce background noise, data were averaged over forward and backward scans and smoothed using a Gaussian filter with a standard deviation of 0.5 pixels (black line). The lateral distance matches that of Supplementary Figure 2(B) (300 pm). (B) E_{diss} data plotted as a function of lateral (x) and vertical (z) tip positions over the red line in Supplementary Figure 2. The tip height (z) is relative, with z = 0 pm defined as the point where E_{diss} can no longer be measured above the noise floor. In the main text, the maximum values of E_{diss} diss from line scans in (B) were plotted as a function of tip

height to compare energy dissipation across bonds. E_{diss} data were measured with 1 pm height intervals, averaged over multiple datasets for accuracy.

E_{diss} acquired by the driving signals clearly indicates the locations of the bonds. Supplementary Figure 4(A) shows the raw data acquired over the position of the red line indicated in Supplementary Figure 2. At the position of the red arrow, the E_{diss} signal is larger than the noise background. To minimize the noise, data were acquired as two lines along both the backward and forward scanning directions. These four lines of data were then averaged, and the 2D images, as a function of tip height, were filtered using a Gaussian filter with a standard deviation of 0.5 pixels (black line of Supplementary Figure 4 (A)). The filter was applied using a square Gaussian kernel. Supplementary Figure 4(B) shows data acquired as a function of lateral (x) and vertical (z) position of the tip over the area indicated by the red line in Supplementary Figure 2.

The labeled height is relative, where z= 0 pm is defined as the point just before E_{diss} can no longer be measured above the noise floor. E_{diss} begins to appear as a peak over the chemical bond and increases as the tip approaches closer (from green to yellow in Supplementary Figure 4(B)) and decreases at even smaller distances (from yellow to blue). Once the tip gets too close, the CO can no longer snap over with each oscillation cycle, causing E_{diss} to decrease.

To compare the energy dissipation characteristics of different chemical bonds, the data were analyzed by plotting only the maximum values of the line scans shown in Supplementary Figure 4(B) as a function of tip height. E_{diss} was measured with a tip height difference of 1 pm. Multiple datasets were acquired over the same bond.

DFT-based determination of the adlayer structure

Calculations were done using the FHI-aims quantum chemistry code.(*1*) We used the PBE exchange-correlation functional(*2*) and the TS^{surf} van der Waals correction scheme(*3*, *4*). The default tight species settings were employed together with a generalized Monkhorst-Pack k-grid(*5*) with 44 k-points. Furthermore, we use the repeated slab approach, where we approximate the substrate using a slab with 5 layers, which are electrostatically decoupled using the dipole correction(*6*). To perform geometry optimizations, all atoms are relaxed.

The commensurate unit cell for the DFT modelling was taken from Wagner et al.(*7*). Two PTCDA molecules were placed in the unit cell using the geometry suggested by the experiment. To attain the global minimum structure, we perform a geometry optimisation based on this experimental starting geometry. Thereby the molecule as well as the first two layers of the copper substrate were allowed to relax, until the remaining force falls below 0.01 eV/Å on each atom.

Snapping model

The snapping model is an extension of the one we described previously in Ref. (*8*). It is used to calculate both frequency shift and energy dissipation over an oscillation cycle assuming:

- The atoms of the surface are static
- The atoms of the tip are static except for the CO molecule at the apex
- The CO at the apex behaves like a torsional spring

The position of the apex metal atom of the tip is specified. Then the tip oscillates laterally from that point. It does so in space (i.e. not in time) and at each position finds the low-energy position (angle) of the CO at the tip apex based upon its previous position. That is, the CO can

only relax to the local energy minimum, not the global energy minimum. In contrast to our previous model, the CO is allowed to relax in two directions.

During the simulation the metal apex is moved stepwise across the surface. At each step, the CO-tip assumes an equilibrium deflection angle. Then the force resulting only from the interaction of the tip with the surface (and not for the torsion spring) is calculated(*9*). The energy dissipation is then calculated by determining the convolution of the force $F(t)$ acting on the CO-tip with the phase of the oscillation.

A machine-learning model for simulating friction

To computationally determine the energy dissipation, we calculate potential energy surfaces (PES) for the interaction of a CO-molecule with the sample surface. For this purpose, we use a machine-learning model based on Gaussian process regression and radial distance functions, which we have previously employed to describe PESs of organic/inorganic interface systems.(*10*) The training data for these potentials is determined using DFT using the same settings as explained above. Separate PESs were determined for each probed bond. Between 250 and 300 data points were used to train a PES for a given bond. The training data was chosen such that we reached a prediction accuracy (based on a leave-one-out-cross-validation-error root-mean-square-error) of within 2 meV for interaction between the CO-molecule and the sample surface. Supplementary Figure 5 shows a learning curve for the C-C(1) bond.

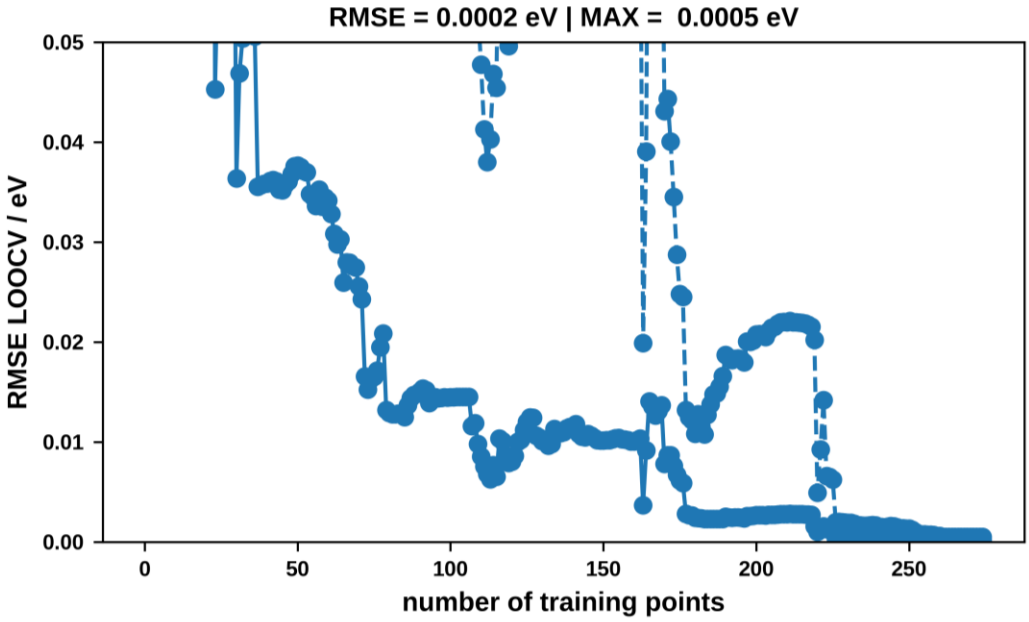

Supplementary Figure 5 | Learning curve for C-C(1) bond showing the leave-one-out-cross-validation-error root-mean-square-error (LOOCV RMSE, solid line) and the maximimum prediction error (dashed line)

We simplify the system by only considering the CO molecule above a free-standing layer of molecules, whereby the geometry of the molecule is the same as adsorbed on a substrate. This simplification is valid since the interaction between the CO-tip and sample is governed by the interaction of the O-atom of the CO molecule with the adsorbate molecule. To demonstrate the validity of our approach, we have additionally determined energy dissipation for the C-C(1), the C-C(3) 4, and the O···H(2) bonds using DFT data that contained the metal substrate below the PTCDA molecule. A comparison between the DFT energy dissipation without substrate, with substrate, and the energy dissipation determined with a commonly used Lennard Jones potential (LJP) is shown in Supplementary Figure 6.

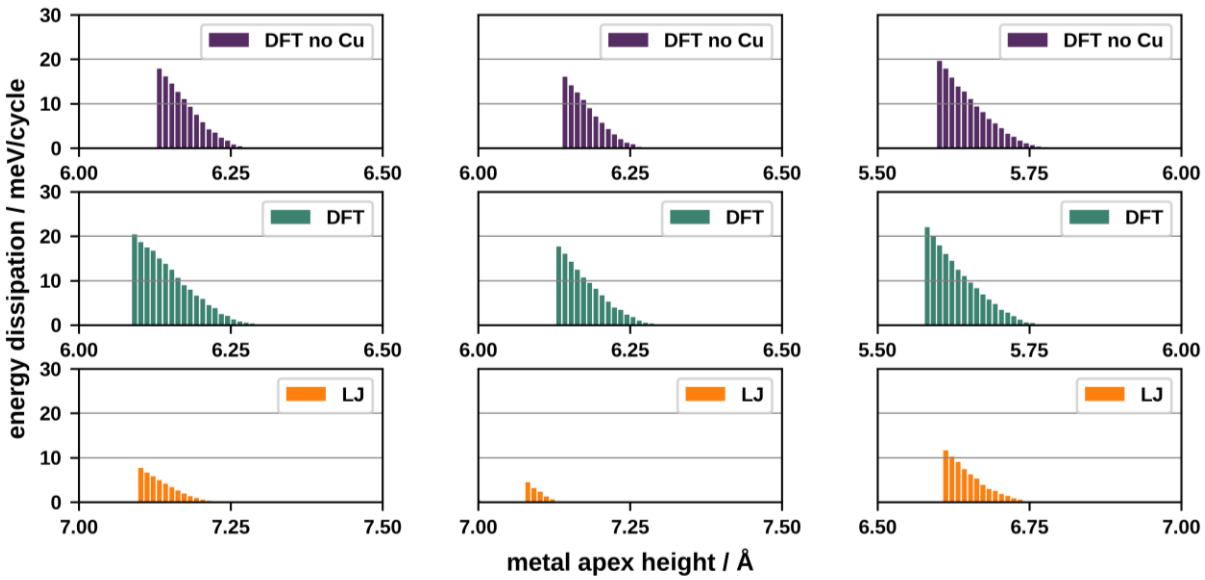

Supplementary Figure 6 | Comparison of energy dissipation calculations using (first row) DFT without a metal substrate, (middle row) DFT with substrate, and (bottom row) a commonly used Lennard Jones potential. First column: CC(1), second column: CC(3), third column: O···H(2)

As shown in Supplementary Figure 6, leaving out the substrate results in a small, constant decrease in energy dissipation. This is a result of attractive, non-site-specific vdW-interactions between the CO-molecule and the substrate, which lead to a lower onset of snapping and thus a slightly larger amount of energy dissipation. Since removing the substrate does not affect the relative amounts of energy dissipation (and only minorly affects the absolute energy dissipation values) we are confident in the validity of our approach. We note in passing that the LJP yields energy dissipation prediction that significantly differs from the DFT results. We attribute this to the more rigorous treatment of the quantum-mechanical interactions between the CO-tip and the PTCDA molecules by DFT. Moreover, this demonstrates the necessity of using accurate first-principles methods if one wishes to determine quantitative predictions of LFM measurements.

Determination of bond order

We determined the bond order using Mulliken population analysis based on the orbital populations calculated using the FHI-aims quantum chemistry code. The FHI-aims quantum chemistry code describes the electronic wave function using a linear combination of atom-centred orbitals based on spherical harmonics and radial function (the latter include cut-offs at large distances).(*11*) The wave function is given by a series expansion in the basis of the atom-centred basis functions:

$$\phi_i = \sum_r c_{ri}\,\chi_r$$

using the series expansion of the wave function, we can determine the total number of electrons by summing over the expansion coefficients c_{ri} and the overlap matrix S_{rs}:

$$N = \sum_i \sum_{r,s} 2\,c_{ri}^{*} c_{si} S_{rs} = \sum_{r,s} P_{rs}\,S_{rs}$$

where we have used $P_{rs} = \sum_i 2\,c_{ri}^{*} c_{si}$. By splitting the summation into sums over all basis function centred on atoms A and B, we can determine the bond order:

$$N = \sum_A \sum_{r,s\in A} P_{rs}\,S_{rs} + \sum_{A<B} 2 \sum_{r\in A}\sum_{s\in B} P_{rs}\,S_{rs} = \sum_A q_A + \sum_{A<B} q_{AB}$$

We can interpret the second contribution q_{AB} as the bond order of the bond between the atoms A and B.

To benchmark this method of bond order determination, we calculate bond orders for simple molecules using identical settings to the calculations presented in the manuscript. Specifically, we compare the C=C double bond in C_2H_4 to the C-C single bond in C_2H_6. The C=C double bond in C_2H_4 has a bond order of 1.35, while the C-C single bond in C_2H_6 has a bond order of 0.71.

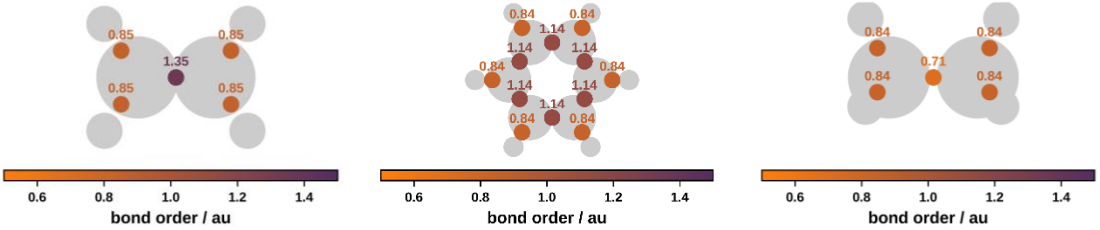

Supplementary Figure 7 | Mulliken bond order for (left) C_2H_4, (middle) C_6H_6, and (right) C_2H_6.

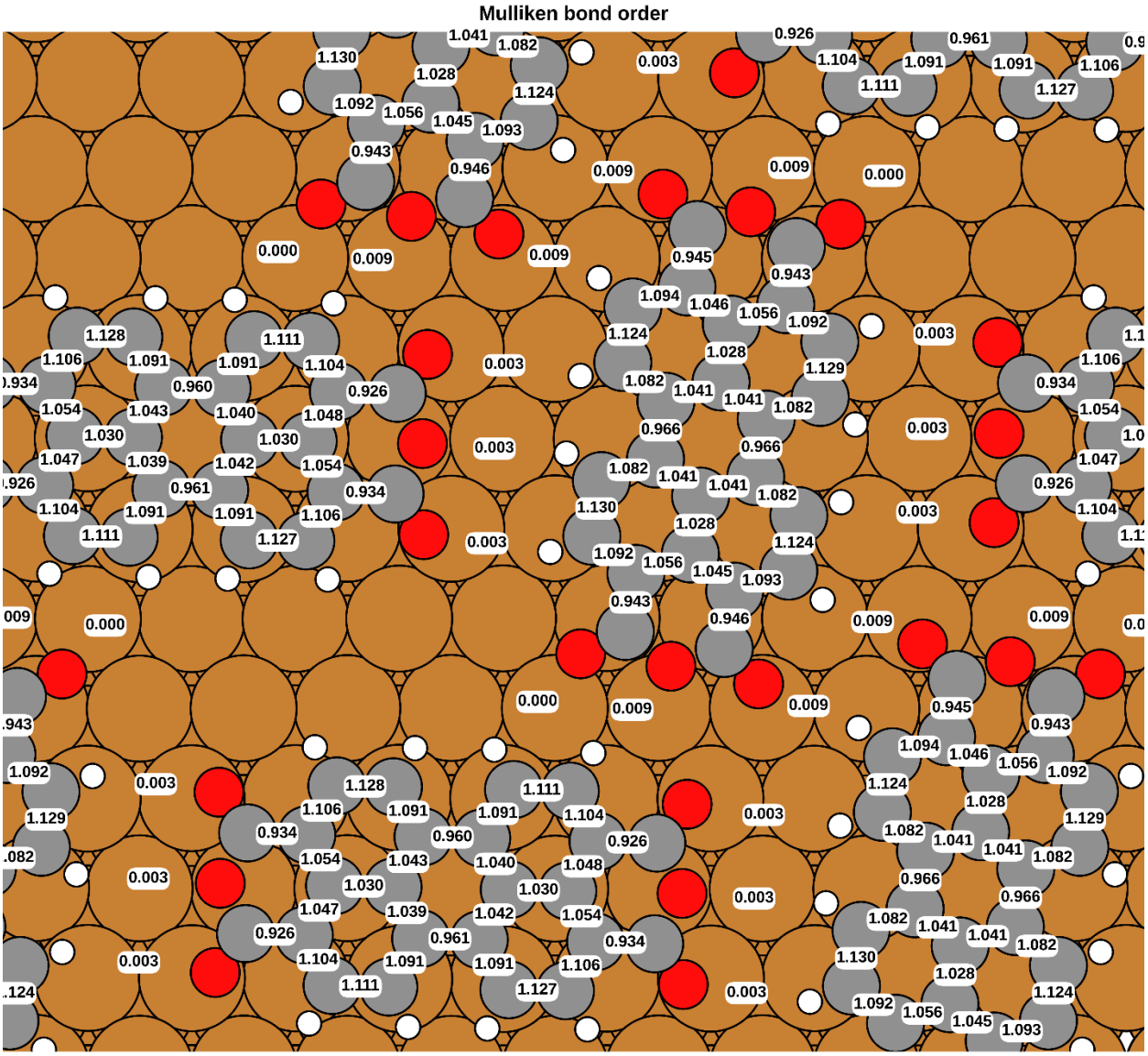

Supplementary Figure 8 | Mulliken bond order of all calculated bonds.

Calculating the correlation and confidence

First we determine the Pearson correlation coefficient r between the bond order and the energy dissipation. For this we find a value of $r = 0.68$. This value indicates a moderate to strong positive linear relationship between the the bond order and the energy dissipation.

To test if the correlation coefficient is meaningful, we use a Student's *t*-test. Here we first calculate t-score:

$$t_{score} = r \cdot \sqrt{\frac{n-2}{1-r^2}}$$

Here n is the sample size and r is the Pearson correlation coefficient. To attain a percentage value for the confidence we evaluate the cumulative distribution function of the Student's *t* using t_{score}. We use a one-tailed test, since we are interested in testing the validity of a positive correlation coefficient. We find a significance of 99.8%. This high significance level means there is a very low probability (0.2%) that the observed correlation is due to random chance.

The potential energy landscape over a covalent versus hydrogen bond

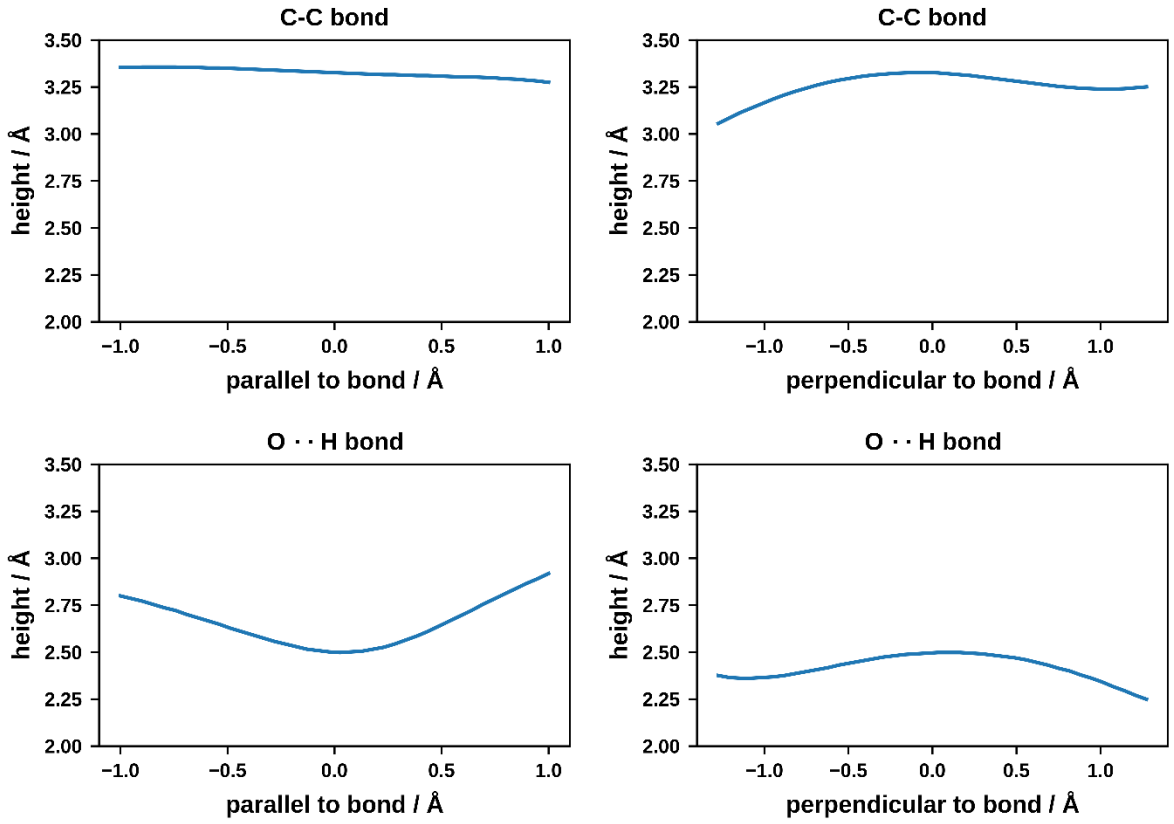

Supplementary Figure 9 | Zero interaction energy isosurface as shown in Fig. 4 e and f. Along the bond (parallel to bond), the shape of the interaction between the two bonds is very different, as the increased electron density between the atoms influences friction only for the covalent bond. Perpendicular to the bond, the energy landscape is similar, which explains the similar magnitude of sliding friction over covalent and hydrogen bonds.

References

1. V. Blum, R. Gehrke, F. Hanke, P. Havu, V. Havu, X. Ren, K. Reuter, M. Scheffler, Ab initio molecular simulations with numeric atom-centered orbitals. *Comput. Phys. Commun.* **180**, 2175–2196 (2009).
2. J. P. Perdew, K. Burke, M. Ernzerhof, Generalized gradient approximation made simple. *Phys. Rev. Lett.* **77**, 3865–3868 (1996).
3. V. G. Ruiz, W. Liu, E. Zojer, M. Scheffler, A. Tkatchenko, Density-functional theory with screened van der Waals interactions for the modeling of hybrid inorganic-organic systems. *Phys. Rev. Lett.* **108**, 146103 (2012).
4. A. Tkatchenko, M. Scheffler, Accurate molecular van der Waals interactions from ground-state electron density and free-atom reference data. *Phys. Rev. Lett.* **102**, 6–9 (2009).
5. J. Moreno, J. M. Soler, Optimal meshes for integrals in real- and reciprocal-space unit cells. *Phys. Rev. B.* **45**, 13891–13898 (1992).
6. J. Neugebauer, M. Scheffler, Adsorbate-substrate and adsorbate-adsorbate interactions of Na and K adlayers on Al(111). *Phys. Rev. B.* **46**, 16067–16080 (1992).
7. T. Wagner, A. Bannani, C. Bobisch, H. Karacuban, R. Möller, The initial growth of PTCDA on Cu(111) studied by STM. *J. Phys. Condens. Matter*. **19**, 056009 (2007).
8. A. J. Weymouth, E. Riegel, O. Gretz, F. J. Giessibl, Strumming a Single Chemical Bond. *Phys. Rev. Lett.* **124**, 196101 (2020).
9. P. Hapala, G. Kichin, C. Wagner, F. S. Tautz, R. Temirov, P. Jelínek, Mechanism of high-resolution STM/AFM imaging with functionalized tips. *Phys. Rev. B.* **90**, 085421 (2014).
10. L. Hörmann, A. Jeindl, O. T. Hofmann, From a bistable adsorbate to a switchable interface: tetrachloropyrazine on Pt(111). *Nanoscale*. **14**, 5154–5162 (2022).
11. V. Blum, R. Gehrke, F. Hanke, P. Havu, V. Havu, X. Ren, K. Reuter, M. Scheffler, Ab initio molecular simulations with numeric atom-centered orbitals. *Comput. Phys. Commun.* **180**, 2175–2196 (2009).